Korea-Australia Rheology Journal
Vol. 19, No. 4, December 2007 pp. 211-219

Numerical result of complex quick time behavior of viscoelastic fluids in flow domains with traction boundaries

Youngdon Kwon*
Department of Textile Engineering, Sungkyunkwan University, Suwon, Kyunggi-do 440-746, Korea
(Received September 10, 2007; final revision received October 30, 2007)

Abstract

Here we demonstrate complex transient behavior of viscoelastic liquid described numerically with the Leonov model in straight and contraction channel flow domains. Finite element and implicit Euler time integration methods are employed for spatial discretization and time marching. In order to stabilize the computational procedure, the tensor-logarithmic formulation of the constitutive equation with SUPG and DEVSS algorithms is implemented. For completeness of numerical formulation, the so called traction boundaries are assigned for flow inlet and outlet boundaries. At the inlet, finite traction force in the flow direction with stress free condition is allocated whereas the traction free boundary is assigned at the outlet. The numerical result has illustrated severe forward-backward fluctuations of overall flow rate in inertial straight channel flow ultimately followed by steady state of forward flow. When the flow reversal occurs, the flow patterns exhibit quite complicated time variation of streamlines. In the inertialess flow, it takes much more time to reach the steady state in the contraction flow than in the straight pipe flow. Even in the inertialess case during startup contraction flow, quite distinctly altering flow patterns with the lapse of time have been observed such as appearing and vanishing of lip vortices, coexistence of multiple vortices at the contraction corner and their merging into one.

Keywords : Leonov model, startup viscoelastic flow, contraction, traction boundary

1. Introduction

Viscoelastic liquids demonstrate various flow behaviors distinct from the Newtonian fluid, most of which result from nonlinear characteristics as well as elasticity of the liquids such as shear thinning and extensional hardening.

Peculiar non-Newtonian flow behavior occurs almost always at high Deborah number or at high flow rate where nonlinear effects dominate. Thus in order to analyze it, one has to perform successful numerical modeling of this high Deborah number flow, which has been a formidable task in the field of computational viscoelastic fluid dynamics. Its difficulty may be expressed via lack of proper mesh convergence, solution inaccuracy and violation of positive definiteness of the conformation tensor (violation of strong ellipticity of partial differential equations), which ultimately result in degradation of the whole numerical scheme. Here again we employ in the finite element formulation the tensor-logarithmic transform, which has been first suggested by Fattal and Kupferman (2004) and has also been applied in our previous works (Kwon, 2004; Yoon and Kwon, 2005). It forbids the violation of positive definiteness of the conformation tensor and therefore eradicates one fatal pathological behavior of governing equations.

The first finite element implementation of this new formalism has been performed by Hulsen (2004) and Hulsen and coworkers (2005), who have demonstrated dramatic stabilization of the numerical procedure with the Giesekus constitutive equation. Kwon (2004) and Yoon and Kwon (2005) have given numerical results of the flow modeling in the domain with sharp corners. In comparison with the conventional method, stable computation has been demonstrated even in this flow domain with sharp corners. In the papers, it has been concluded that this new method may work only for constitutive equations proven globally stable.

The time-dependent viscoelastic flow modeling has been performed mainly by implementing hybrid finite element/finite volume method. Sato and Richardson (1994) have observed heavy oscillations of the centerline velocity in the inertial straight channel flow of the upper convected Maxwell liquid when the traction boundary condition is assigned at the inlet and outlet boundaries. The numerical results obtained by Webster and coworkers (2004) illustrate quite distinct time variation of transient streamlines as well as fluctuations of rheological variables in the planar con-

*Corresponding author: kwon@skku.edu

traction flows. With the stabilizing tensor-logarithmic formulation, Fattal and Kupferman (2005) have also executed time-dependent simulation of the lid-driven cavity flow with the Oldroyd-B model. In fact, their tensor-logarithmic formulation does not allow direct computation for the steady state due to complicated logarithmic transform involved in the formulation.

In this work, we consider the viscoelastic time-dependent flows in a planar straight and 4 : 1 contraction channels with traction boundaries specified at the inlet and outlet of the pipe instead of flow velocity profiles.

2. Equations in 2D planar flow

In order to describe dynamic flow behavior of incompressible fluids, we first require the equation of motion and continuity equation

$$\rho\left(\frac{\partial \mathbf{v}}{\partial t}+\mathbf{v}\cdot\nabla\mathbf{v}\right)=-\nabla p+\nabla\cdot\tau, \quad \nabla\cdot\mathbf{v}=0. \tag{1}$$

Here ρ is the density of the liquid, $\mathbf{v}$ the velocity, τ the extra-stress tensor. and p is the pressure. The gravity force is neglected in the analysis and ∇ is the usual gradient operator in tensor calculus. When kinematic relation of the extra-stress is specified in terms of the constitutive model, the set of governing equations becomes complete for isothermal incompressible viscoelastic flows.

In expressing viscoelastic property of the liquid, the Leonov constitutive equation (Leonov, 1976) is employed, since it may be the only model that can successfully describe highly elastic flow phenomena with robust computational stability. The differential viscoelastic constitutive equations derived by Leonov can be written into the following quite general form:

$$\tau=(1-s)G\left(\frac{I_1}{3}\right)^n\mathbf{c}+2\eta s\mathbf{e}, \quad W=\frac{3G}{2(n+1)}\left[\left(\frac{I_1}{3}\right)^{n+1}-1\right],$$

$$\mathbf{e}=\frac{1}{2}(\nabla\mathbf{v}+\nabla\mathbf{v}^T),$$

$$\frac{d\mathbf{c}}{dt}-\nabla\mathbf{v}^T\cdot\mathbf{c}-\mathbf{c}\cdot\nabla\mathbf{v}+\frac{1}{2\theta}\left(\frac{I_1}{I_2}\right)^m\left(\mathbf{c}^2+\frac{I_2-I_1}{3}\mathbf{c}-\delta\right)=\mathbf{0}. \tag{2}$$

Here $\mathbf{c}$ is the elastic strain tensor that explains elastic strain accumulation in the Finger measure during flow, $\frac{d\mathbf{c}}{dt}=\frac{\partial\mathbf{c}}{\partial t}+\mathbf{v}\cdot\nabla\mathbf{c}$ is the total time derivative of $\mathbf{c}$, $\frac{d\mathbf{c}}{dt}-\nabla\mathbf{v}^T\cdot\mathbf{c}-\mathbf{c}\cdot\nabla\mathbf{v}$ is the upper convected time derivative, G is the modulus, θ is the relaxation time, $\eta=G\theta$ is the total viscosity that corresponds to the zero-shear viscosity and s is the retardation parameter that specifies the solvent viscosity contribution. The tensor $\mathbf{c}$ reduces to the unit tensor δ in the rest state and this also serves as the initial condition in the start-up flow from the rest. In the asymptotic limit of $\theta\rightarrow\infty$ where the material exhibits purely elastic behavior, it becomes the total Finger strain tensor.

$I_1=\mathrm{tr}\mathbf{c}$ and $I_2=\mathrm{tr}\mathbf{c}^{-1}$ are the basic first and second invariants of $\mathbf{c}$, respectively, and they coincide in planar flows. Due to the characteristic of the Leonov model, the third invariant I_3 satisfies specific incompressibility condition such as $I_3=\det\mathbf{c}=1$. In addition to the linear viscoelastic parameters, it contains 2 nonlinear constants m and n ($n>0$), which can be determined from simple shear and uniaxial extensional flow experiments. They control the strength of shear thinning and extension hardening of the liquid. However the value of the parameter m does not have any effect on the flow characteristics here in 2D situation, since two invariants are identical. Thus in this study we adjust only the parameter n to attain appropriate (planar) extension hardening characteristic. The total stress tensor is obtained from the elastic potential W based on the Murnaghan's relation. Since the extra-stress is invariant under the addition of arbitrary isotropic terms, when one presents numerical results it may be preferable to use $\tau=(1-s)G\left(\frac{I_1}{3}\right)^n(\boldsymbol{c}-\delta)+2\eta s\mathbf{e}$ instead in order for the stress to vanish in the rest state.

The essential idea presented by Fattal and Kupferman (2004) in reformulating the constitutive equations is the tensor-logarithmic transformation of $\mathbf{c}$ as follows:

$$\mathbf{h}=\log\mathbf{c}. \tag{3}$$

Here the logarithm operates as the isotropic tensor function, which implies the identical set of principal axes for both $\mathbf{c}$ and $\mathbf{h}$. In the case of the Leonov model, this $\mathbf{h}$ becomes another measure of elastic strain, that is, twice the Hencky elastic strain. While $\mathbf{c}$ becomes δ, $\mathbf{h}$ reduces to $\mathbf{0}$ in the rest state.

In the case of 2D planar flow, the final set of the Leonov constitutive equations in the $\mathbf{h}$-form has its closed form and it has been given in (Kwon, 2004; Yoon and Kwon, 2005). Actually the total set of eigenvalues in this 2D flow is h, $-h$ and 0. In the notation of the $\mathbf{h}$ tensor the incompressibility relation $\det\mathbf{c}=1$ becomes

$$\mathrm{tr}\mathbf{h}=0. \tag{4}$$

In this 2D analysis, $h_{11}=-h_{22}$, $h_{33}=0$ and thus the viscoelastic constitutive equations add only 2 supplementary unknowns such as h_{11} and h_{12} to the total set of variables.

3. Numerical procedure and boundary conditions

The geometric details of the flow domains in straight and 4 : 1 contraction channels are illustrated in Fig. 1. Since we are employing the traction boundaries at the inlet and outlet of the flow with stress free condition ($\mathbf{h}=\mathbf{0}$) at the inlet, relatively long upstream and downstream channels are necessary to effectively remove the disturbances introduced by the actually unknown stress boundary conditions. However the length of the channels that may not be long enough to

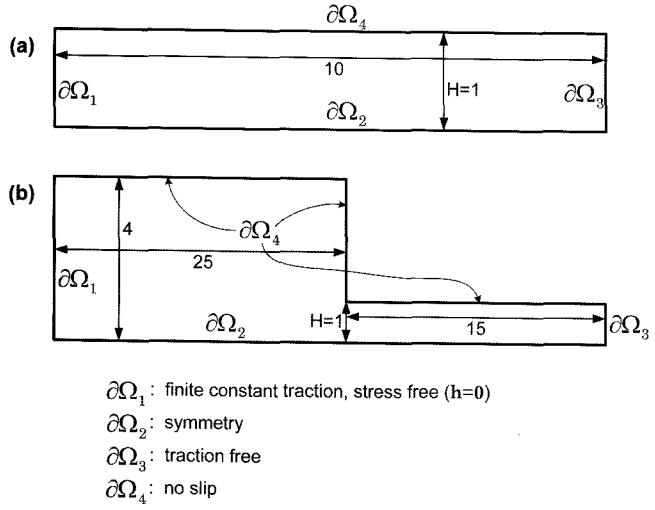

Fig. 1. Schematic diagram of the problem domain for the flow in (a) straight and (b) 4:1 contraction channels.

guarantee the accuracy of numerical results, is employed as in the Fig. 1 to compromise the accuracy with the heavy computational load in this time-dependent viscoelastic flow modeling. A more detailed discussion follows afterwards.

All the computational scheme except for the boundary conditions is identical with the one employed in the previous studies (Kwon, 2004; Yoon and Kwon, 2005). With the standard Galerkin formulation adopted as basic computational framework, streamline-upwind/Petrov-Galerkin (SUPG) method as well as discrete elastic viscous stress splitting (DEVSS) (Guénette and Fortin, 1995) algorithm is implemented. The upwinding algorithm developed by Gupta (1997) has been applied.

As for the time integration of the evolution and momentum equations, the implicit Euler method is applied. Even though the time marching is only the 1st order in accuracy, the computational load is quite heavy since it is fully implicit and at every time step the values of the whole set of nodal variables can be obtained only by solving the complete linear system. The time steps have been manually adjusted to preserve the stability and also to save the computation time, and they are in the range of $10^{-3}\sim10^{-5}\times\theta$.

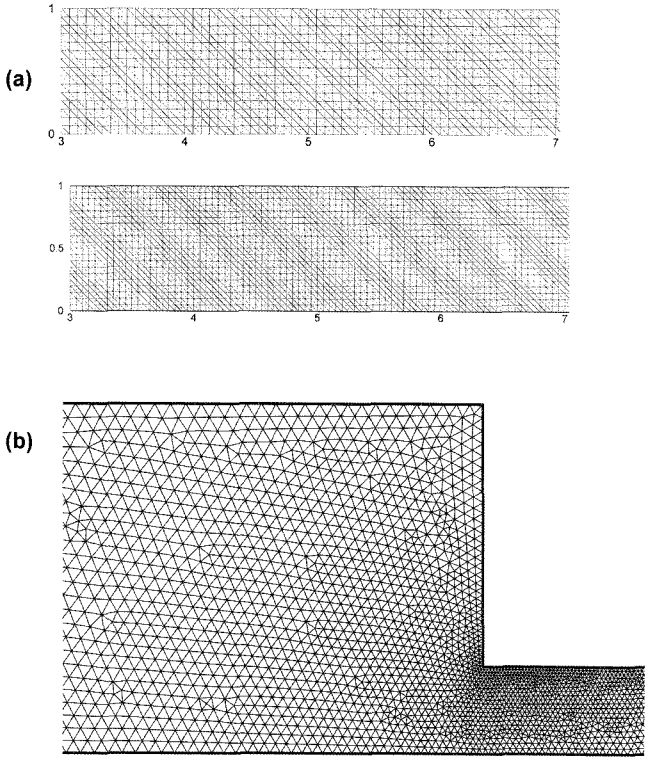

Fig. 2. Partial view of the meshes employed in the computation. (a) coarse and fine meshes for a straight channel; (b) a mesh for a 4:1 contraction channel.

2 types of structured mesh for the straight channel and 1 of unstructured mesh for the contraction channel are employed and their partial views are illustrated in Fig. 2. Corresponding mesh details are given in Table 1. The flow problem through the straight channel has been chosen in order to investigate the proper mesh convergence as well as to study complex nonlinear flow behavior. Thus the structured meshes are employed in the study of the straight pipe flow to avoid artificial numerical error possibly introduced via non-uniform space discretization. For the analysis of the contraction flow, the finest mesh elements are located near the contraction corner where numerical singularity occurs.

Table 1. Characteristics of the 2 meshes employed in the computation

	Length of the side of the smallest element	No. of elements	No. of linear nodes	No. of quadratic nodes	No. of unknowns
Straight channel - Coarse mesh (structured)	1/15	4,500 (15×150×2)	2,416	9,331	46,988
Straight channel - Fine mesh (structured)	1/20	8,000 (20×200×2)	4,221	16,441	82,648
4:1 contraction channel (unstructured)	0.035	11,006	5,824	22,653	113,908

Linear for pressure and strain rate and quadratic interpolations for velocity and **h**-tensor are applied for spatial continuation of the variables. In order to mimic dimensionless formulation, we simply assign unit values for G and θ (Hence the zero-shear viscosity $\eta = G\theta$ also becomes unit) and adjust the Deborah number (or the Reynolds number) by the variation of the average flow rate (actually by varying the traction force at the inlet of the channel) for steady state computation. In the case of transient viscoelastic flow with constant traction forces, the flow rate varies with time and thus the Deborah and Reynolds numbers are also time-dependent.

In order to solve the large nonlinear system of equations introduced, the Newton iteration is used in linearizing the system. As an estimation measure to determine the solution convergence, the L_∞ norm scaled with the maximum value of the nodal variables in the computational domain is employed. Hence when the variation of every nodal variable in the Newton iteration does not exceed 10^{-4} of its value in the previous iteration, the algorithm concludes that the converged solution is attained. For the viscoelastic variables, we examine the relative error in terms of the eigenvalue of the **c**-tensor. We have found that this convergence criterion imposes less stringent condition on the computational procedure, and this criterion seems quite practical and appropriate since we mainly observe the results in terms of physically meaningful **c**-tensor or stress rather than **h**.

Here we adopt the traction boundary condition. First all the components of traction vanish at the outlet. On the other hand, in the flow direction (x-axis) at the inlet, the constant finite traction force is applied in terms of dimensionless value of t_x/G where t_x the surface traction (force per unit area) in the x-direction. In the transverse direction (y-axis), we set the boundary free from the traction force. Since the evolution equation of **h**-tensor is of hyperbolic type, we need to specify its values at the inlet boundary, which play the role of initial conditions for the start of the characteristic curves or cones. However those inlet boundary values of **h**-tensor are not known. Here we simply specify zero values for all components of **h**-tensor (stress free condition) at the inlet, which requires some justification for this rather arbitrary assignment. First this type of boundary means that the region outside the inlet boundary is considered to be a zero stress reservoir just like pressure or heat reservoir in thermodynamics. In practice, the length of the upstream channel has to be long enough to eliminate the effect of this zero stress boundary. However in this study, especially in the modeling of straight channel flow, the pipe length is rather short to cut down the computational burden, and we simply regard the region outside the flow domain as the zero stress reservoir.

Certainly one may employ the traction boundary condition obtained from the analytic solution for the fully developed flow along the straight pipe. However it is applicable only for 2D or axisymmetric case, since in the general 3D fully developed flow the analytic solution for the channel with an arbitrary cross-section is not known and has to be obtained again numerically. Even in the 2D startup flow, the boundary condition is not known, since it is also time-dependent and highly oscillatory in general. Hence in the current flow analysis we implement the simple condition of zero stress other than the fully developed flow alternative.

4. Results and Discussion

This study mainly focuses on illustrating possible complexity in time-dependent flow numerically described by the viscoelastic constitutive equations, here specifically by the Leonov model. However before explaining the main results, it is worthwhile to mention the accuracy and the stability characteristics of the current numerical scheme augmented by the tensor-logarithmic transformation (3).

Although the detailed result is not presented in this paper, we have found in the previous works (Kwon, 2004; Yoon and Kwon, 2005) proper characteristics of mesh convergence for the tensor-logarithmically transformed formulation. Since we have adopted not the boundary condition with velocity profile specified but the traction boundaries both at the inlet and outlet, there may exist numerical artifact that the flow rate at the inlet differs from that at the outlet if the incompressibility condition is not appropriately accounted in the computation domain. However the computational results have shown that the flow rates at the inlet and outlet coincide up to the 13th significant digit for both straight and contraction pipe flows.

We define the dimensionless flow rate by the Deborah number as

$$De = \frac{U\theta}{H}. \tag{5}$$

where U is the average flow rate at the channel outlet and H shown Fig. 1 is the width of the downstream channel. Since we have chosen the valule of 1 for θ and H, the Deborah number is identical with the average flow rate U or the total flow rates both at the inlet and outlet. As the Newtonian viscous term becomes relatively large, the stability of the system is dramatically improved. When we specify $s=0.01$ with $n=0.1$ and $\rho=0\sim0.01$ (here the density ρ is made dimensionless with $\frac{G\theta^2}{H^2}$) for the Leonov model (4), we have obtained the stable solution over $De=300$ ($t_x/G\approx300$) and stopped the computation due to no further interest. This result of stability at extremely high Deorah number agrees with results obtained in the previous works (Hulsen, 2004; Hulsen *et al.*, 2005). However when s becomes 0.001, the limit Deborah number, over which sta-

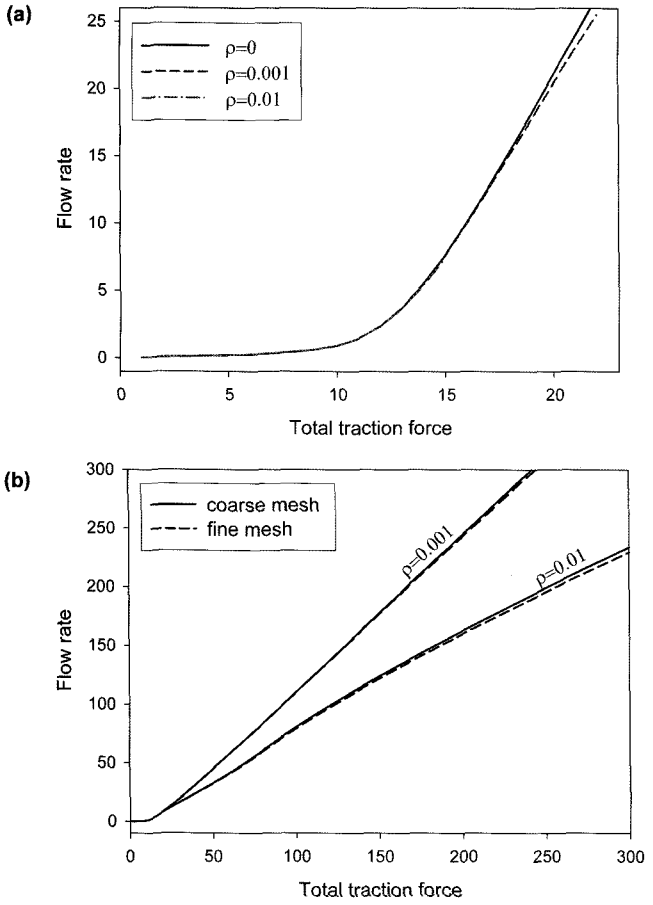

Fig. 3. The flow rate (the Deborah number) vs. traction force with $n=0.1$ in the straight channel flow. (a) $s=0.001$ and (b) $s=0.01$.

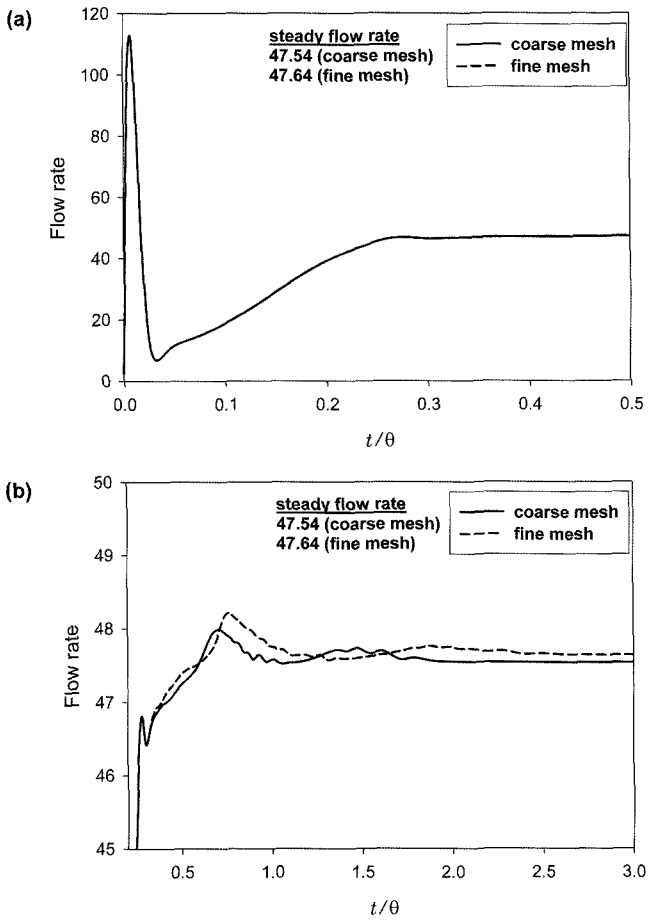

Fig. 4. (a) The flow rate (the Deborah number) as a function of time, and (b) the flow rate curve with enlarged y-axis ($t_x/G=50$, n=0.1, $s=0.01$, $\rho=0.0001$).

ble computation cannot be carried out, becomes finite in the range of 6~30, the exact value of which depends on the density.

In Fig. 3, one can observe the dependence of the steady flow rate in terms of the Deborah number on the traction force for $s=0.001$ and $s=0.01$ with various density in straight channel flow. Fig. 3(b) also shows the comparison of results for 2 different structured meshes, where quite close coincidence may be observed.

Fig. 4 illustrates fluctuation of the time-dependent flow rate for $t_x/G=50$, s=0.01 and $\rho=0.0001$. Even though we can observe almost no difference between results of coarse and fine meshes, in the enlarged view of Fig. 4(b) the solution starts to deviate at $t/\theta\approx0.4$ and the values of steady flow rate exhibit about 0.2% discrepancy. However we neglect possible lack of mesh refinement and from now on we only present results for the coarse mesh spatial discretization in order to lessen heavy computational load.

One can examine quite dramatic difference in the flow behavior exhibited by inertia in Fig. 5 when the Newtonian viscous effect is low ($s=0.001$). For $t_x/G=5$ and for all values of density the flow rate is almost identical at 0.202. Whereas the flow rate immediately reaches its steady value for inertialess flow, with small inertial force the flow exhibits highly oscillatory behavior that alternates between forward and even backward directions. This severe fluctuation coincides with the numerical result obtained by Sato and Richardson (1994), who have demonstrated oscillatory centerline velocity in planar Poiseuille flow and compared it with the analytic solution.

Fig. 6 shows streamlines of this flow reversal, where upper 5 figures illustrate a series of changing streamlines from forward to backward and lower 4 exhibit backward to forward reversal. One can see the variation of overall flow rate in terms of the Deborah number. In comparison with the total period of flow, the duration of these complicated flow patterns caused by the flow reversal is quite short. The last one in Fig. 6 corresponds to the streamlines at t/θ=10, when the flow rate De becomes 0.202. Then the flow has almost reached its steady state. The straight streamlines in the whole domain except in the vicinity of inlet and outlet can be seen, which indirectly shows the evidence for the development of the fully developed flow, and the disturbance introduced by the inlet traction bound-

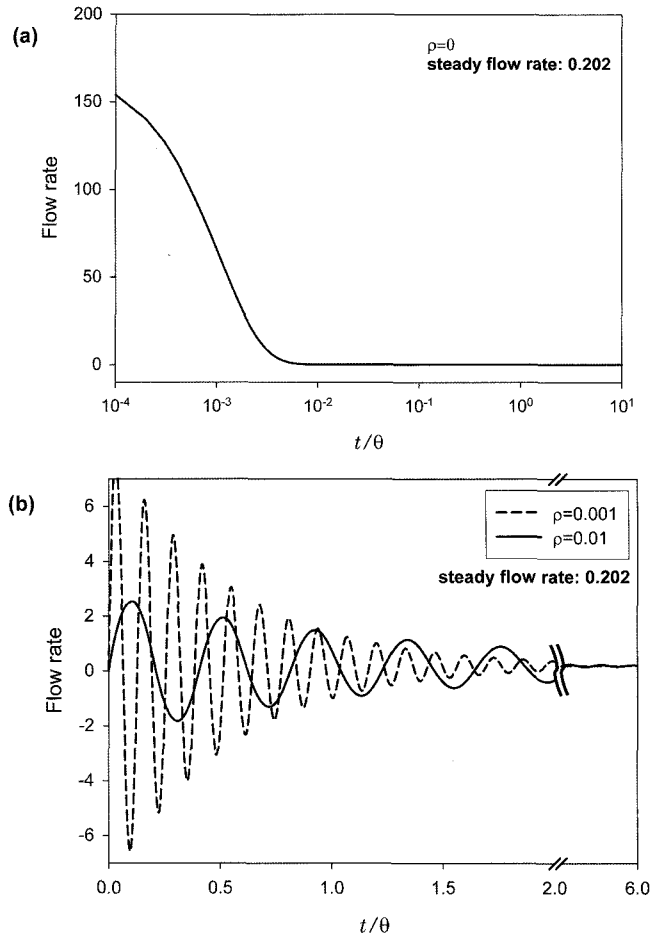

Fig. 5. The flow rate (the Deborah number) as a function of time ($t_x/G=5$, n=0.1, $s=0.001$). (a) ρ=0 with time in logarithmic scale and (b) ρ=0.001, ρ=0.01 in linear time scale.

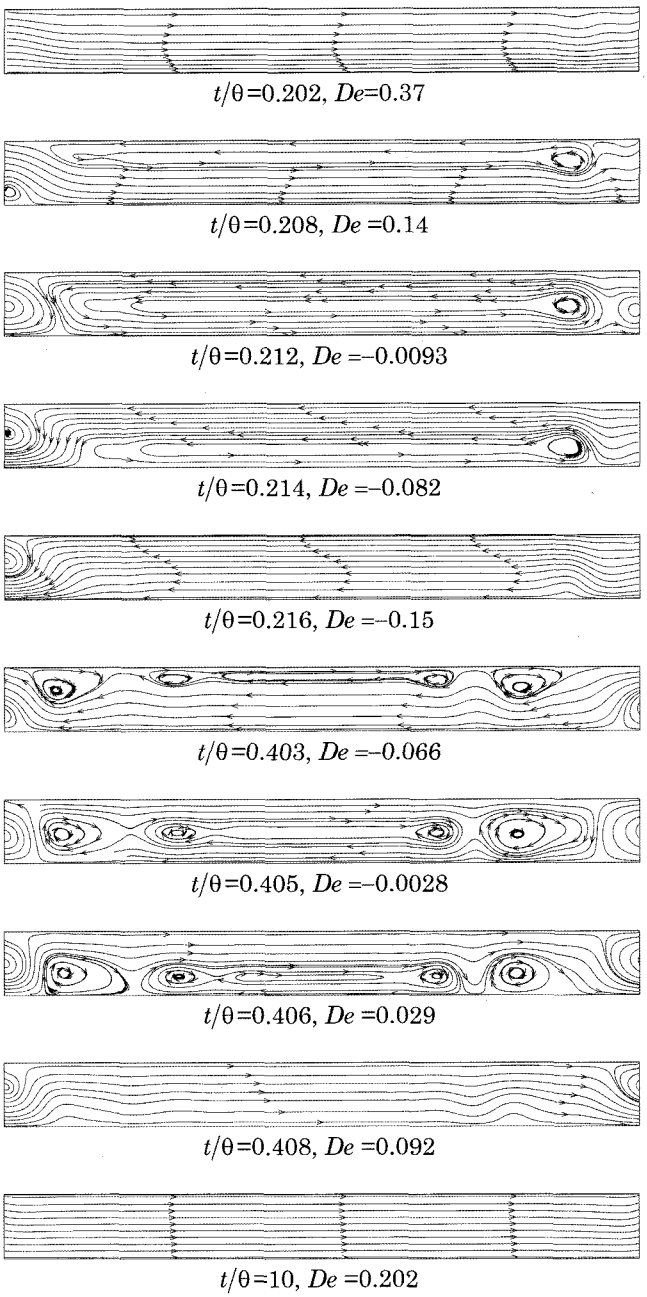

Fig. 6. Streamlines of the straight channel flow ($tx/G=5$, $n=0.1$, $s=0.001$, ρ=0.01) during the period of flow reversal and for the steady state (the last one).

ary exhibited by the curved streamlines damps out immediately.

In Fig. 7, the steady flow curves (flow rate vs. total traction force $4t_x/G$) are depicted for inertialess and low Reynolds number flows in 4 : 1 contraction channel. Due to the shear thinning characteristic of the liquid, the slopes of all curves increase with the traction force. As the Reynolds number (here ρ) increases, the overall flow rate decreases since certain portion of the pressure force has to be allocated for inertia, *i.e.*, for moving mass of liquid. In the case of contraction flow that contains singular point in the computation domain, there exists some limit of the Deborah number, over which stable computation is no longer possible, and such limit decreases with the Reynolds number.

The time variation of startup inertialess contraction flow for $4t_x/G=200$, $n=0.1$, $s=0.001$ is depicted in Fig. 8. In the case of inertialess startup flow (the cases of Fig. 5(a) as well as Fig. 8) the flow rate instantly reaches finite value that corresponds to the flow rate for the Newtonian liquid with viscosity sη. In other words, the fluid velocity discontinuously attains its corresponding Newtonian value from the rest state since there is no inertia by the assumption. Furthermore without the retardation term, that is, $s=0$, the inertialess flow velocity at the startup becomes infinite due to instantaneous elastic deformation made possible from the constitutive modeling for the Maxwellian liquid. The flow rate becomes as low as 3.83 at $t/\theta=0.0125$, the decrease of which results from the elastic recovery of the liquid, and then slowly reaches its steady limit of 50.7 after some fluctuations. In the case of such

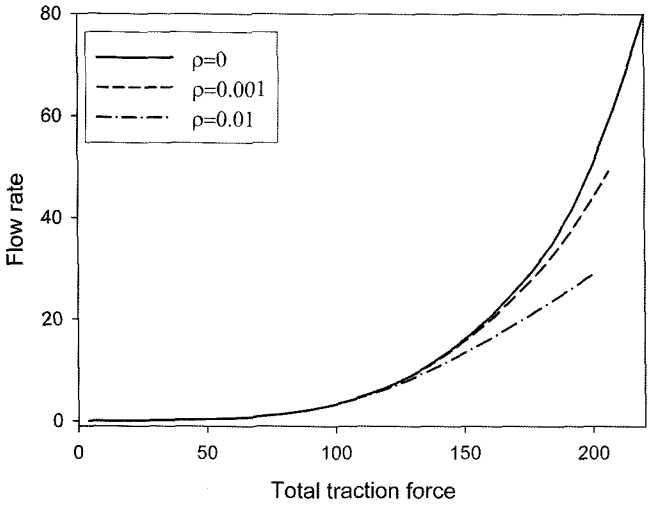

Fig. 7. The flow rate (the Deborah number) vs. total traction force ($4t_x/G$) with n=0.1 and s=0.001 in the 4:1 contraction flow.

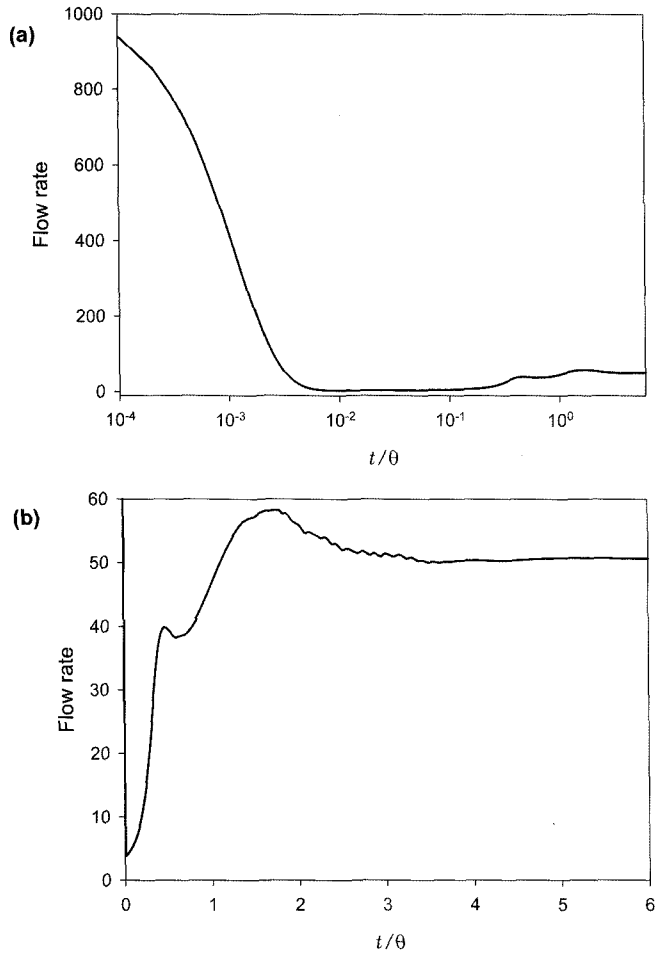

Fig. 8. The flow rate (the Deborah number) as a function of time in the inertialess 4:1 contraction flow ($4t_x/G$=200, n=0.1, s=0.001, ρ=0) (a) in logarithmic time scale and (b) in linear time scale.

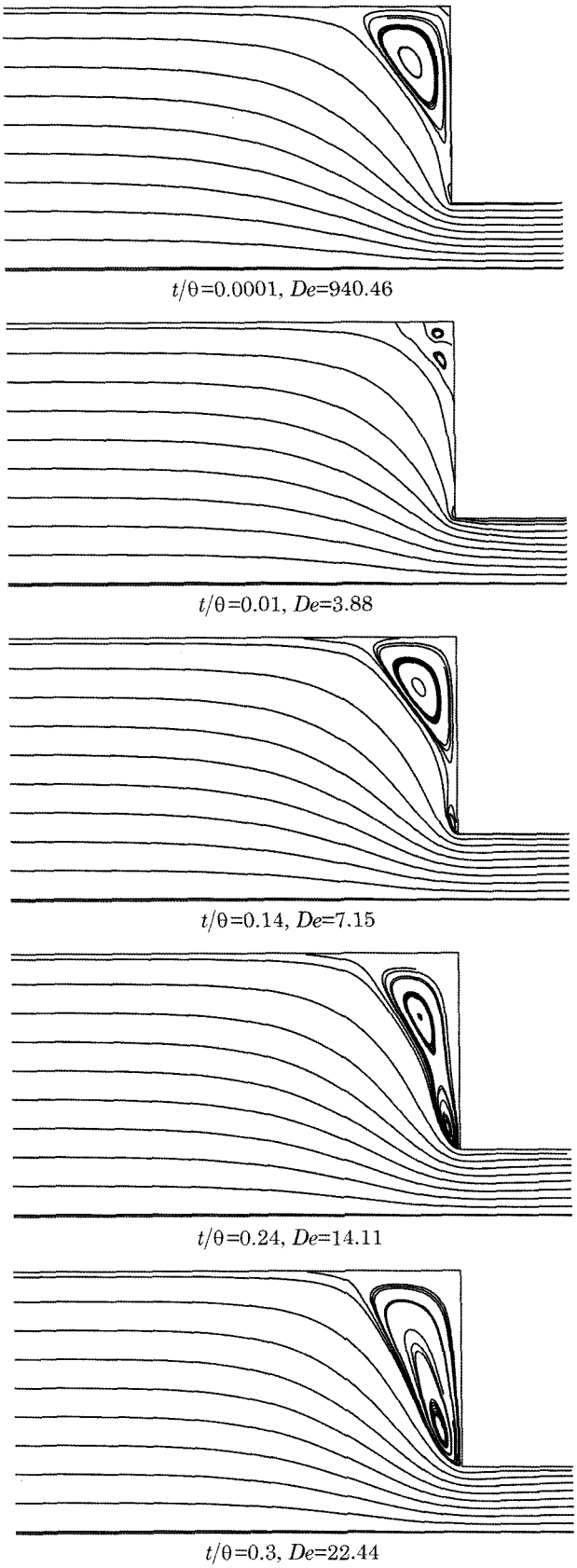

Fig. 9. Streamlines at various time instants for the startup 4:1 contraction flow ($4t_x/G$=200, n=0.1, s=0.001, ρ=0).

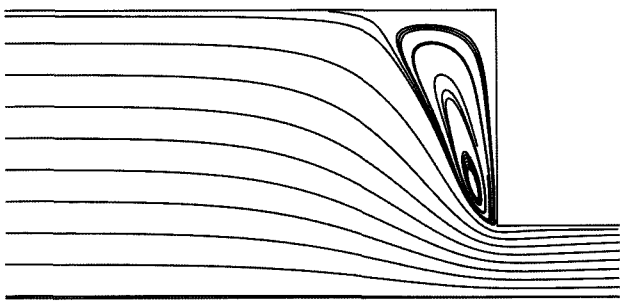

t/θ=0.3, De=22.44

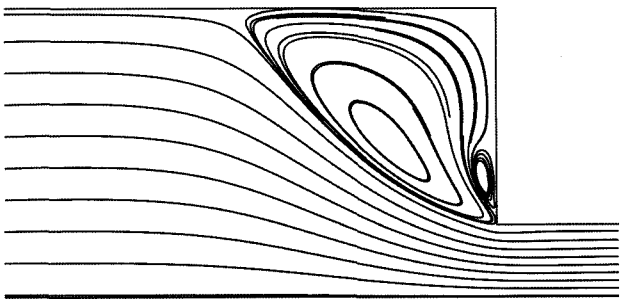

t/θ=0.56, De=38.57

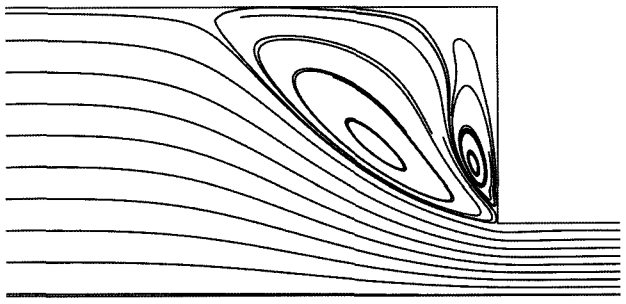

t/θ=0.63, De=38.45

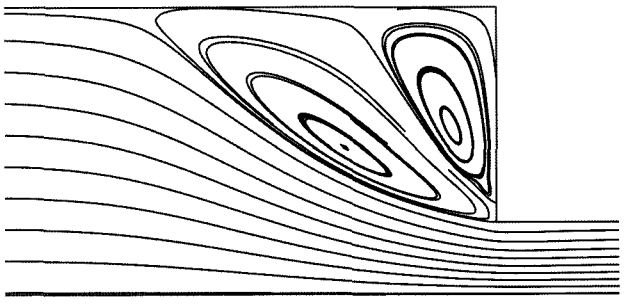

t/θ=0.8, De=40.39

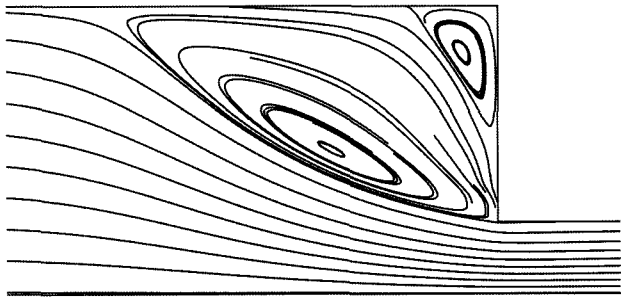

t/θ=1, De=46.41

Fig. 9. Continue.

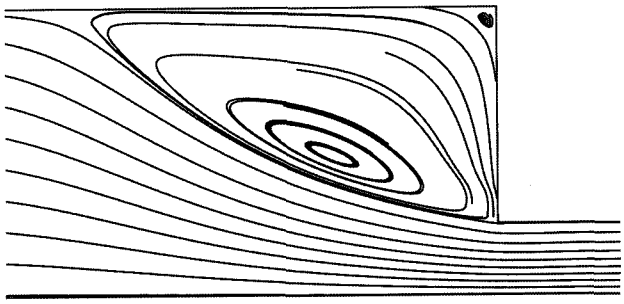

t/θ=1.3, De=55.10

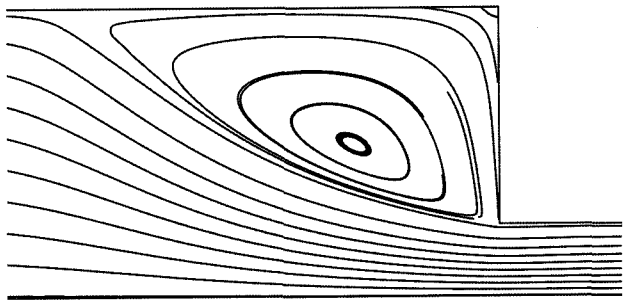

t/θ=6, De=50.68

Fig. 9. Continue.

simple flow geometry as straight channel, the steady state for the inertialess flow can be reached within t/θ=0.01 from the onset of flow. However for more complex flow domain such as the contraction flow, it takes about t/θ=4 to attain its steady state because of intricate rearrangements in the flow field that is clearly demonstrated in the next figure.

Fig. 9 displays a time series of snapshots of streamlines in the inertialess contraction flow under discussion. The first one at t/θ=0.0001 presents streamlines that approximately coincides with those for the inertialess Newtonian flow with viscosity $s\eta$. When the flow rate is nearly the lowest at t/θ=0.0125, the vortex almost disappears possibly due to elastic retraction (slowdown of flow rate caused by elastic recovery). Then the lip vortex in addition to the salient corner vortex appears and afterwards the two vortices are combined (figure at t/θ=0.3) into one which grows in size. At t/θ=0.56 another lip vortex is created and then grows. The coexistent vortices are approximately comparable in size at t/θ=0.8 and then the newly created vortex slowly becomes small and finally disappears. The flow field recomposes the shape of the salient vortex into its steady form and ultimately the steady state is attained.

This complicated transient flow behavior described numerically with the Leonov viscoelastic constitutive equations may be some unrealistic artifact produced by exorbitantly simplified assumptions. In particular, the inlet traction boundary condition may be considered far from real situation. In reality, obtaining the boundary condition that exactly duplicates the genuine system is not possible. One may think of such boundary condition that specifies

fully developed flow profile continuously increasing from the rest to some desired values. Even though such condition may not contain logical flaw, it seems more unrealistic or more remote from the physical system at least to current authors. Actually at this stage the scientist himself has to decide which simplifying assumption introduced in order to make modeling possible is considered to be more reasonable in some or in any sense.

5. Conclusions

In this study, we demonstrate complex transient behavior of viscoelastic liquid described numerically with the Leonov model for straight and contraction channel flow domains. For completeness of computational formulation, the so called traction boundaries are assigned for flow inlet and outlet boundaries. At the inlet, finite traction force in the flow direction with stress free condition is allocated whereas the traction free condition is assigned at the outlet. The numerical result has illustrated severe forward-backward fluctuations of overall flow rate in inertial straight channel flow ultimately followed by steady state of forward flow. When the flow reversal occurs, the flow patterns exhibit quite complicated time variation of streamlines. In the inertialess flow, it takes much more time to reach the steady state in the contraction flow than in the straight pipe flow. Even in the inertialess contraction flow during startup, quite distinct flow patterns have been observed such as coexistence of multiple vortices and their merging into one. Even though the traction boundary restriction imposed in this computational scheme may be considered unrealistic, this work at least demonstrates complicated flow phenomena possible in startup viscoelastic fluid flow.

Acknowledgements

This study was supported by research grants from the Korea Science and Engineering Foundation (KOSEF) through the Applied Rheology Center (ARC), an official KOSEF-created engineering research center (ERC) at Korea University, Seoul, Korea.

References

Fattal, R. and R. Kupferman, 2004, Constitutive laws of the matrix-logarithm of the conformation tensor, *J. Non-Newtonian Fluid Mech.* **123**, 281-285.

Fattal, R. and R. Kupferman, 2005, Time-dependent simulation of viscoelastic flows at high Weissenberg number using the log-conformation representation, *J. Non-Newtonian Fluid Mech.* **126**, 23-37.

Gupta, M., 1997, Viscoelastic modeling of entrance flow using multimode Leonov model, *Int. J. Numer. Meth. Fluids* **24**, 493-517.

Hulsen, M. A., 2004, *Keynote presentation in Internatioan Congress on Rheology 2004*, Seoul, Korea.

Hulsen, M. A., R. Fattal and R. Kupferman, 2005, Flow of viscoelastic fluids past a cylinder at high Weissenberg number: Stabilized simulations using matrix logarithms, *J. Non-Newtonian Fluid Mech.* **127**, 27-39.

Kwon, Y., 2004, Finite element analysis of planar 4:1 contraction flow with the tensor-logarithmic formulation of differential constitutive equations, *Korea-Australia Rheology J.* **16**, 183-191.

Leonov, A. I., 1976, Nonequilibrium thermodynamics and rheology of viscoelastic polymer media, *Rheol. Acta* 15, 85-98.

Sato, T. and M. Richardson, 1994, Explicit numerical simulation of time-dependent viscoelastic flow problems by a finite element/finite volume method, *J. Non-Newtonian Fluid Mech.* **51**, 249-275.

Webster, M. F., H. R. Tamaddon-Jahromi and M. Aboubacar, 2004, Transient viscoelastic flows in planar contractions, *J. Non-Newtonian Fluid Mech.* **118**, 83-101.

Yoon, S. and Y. Kwon, 2005, Finite element analysis of viscoelastic flows in a domain with geometric singularities, *Korea-Australia Rheology J.* **17**, 99-110.